Dehydrogenation of ethylbenzene with CO_2 over Cr-MCM-41 catalyst

Yoshihiko Ohishi[a], Tomonori Kawabata[a], Tetsuya Shishido[b], Ken Takaki[a],
Qinghong Zhang[c], Ye Wang[c], Katsuomi Takehira[a],*

[a] *Department of Chemistry and Chemical Engineering, Graduate School of Engineering, Hiroshima University,
Kagamiyama 1-4-1, Higashi-Hiroshima 739-8527, Japan*
[b] *Department of Chemistry, Tokyo Gakugei University, Nukui-kita 4-1-1, Koganei, Tokyo 184-8501, Japan*
[c] *State Key Laboratory for Physical Chemistry of Solid Surfaces, Department of Chemistry, Xiamen University, Xiamen 361005, China*

Abstract

M-MCM-41 catalysts (M: V, Cr, Fe, and Ga) prepared by direct hydrothermal synthesis (DHT) have been tested for dehydrogenation of ethylbenzene with CO_2. The synthesized materials were characterized by X-ray diffraction (XRD), N_2 adsorption (77 K), and diffuse reflectance UV–vis spectroscopic measurements. Cr-MCM-41 showed the highest activity among M-MCM-41 catalysts tested, resulting in the production of styrene with the conversion of 65% and the selectivity above 90%. The rate of styrene formation increased with increasing Cr loading up to 1.7 wt.%. It is suggested that $Cr(VI)O_4$ in tetrahedral coordination is formed as an active monochromate species and reduced to $Cr(III)O_6$ in octahedral coordination as a less active polychromate species during the reaction. Deactivated catalyst was regenerated by a treatment with gaseous oxygen or CO_2, during which redistribution as well as reoxidation of polymeric $Cr(III)O_6$ octahedra to monomeric $Cr(VI)O_4$ tetrahedra was observed. The rate of CO formation increased together with that of styrene formation, while the rate of H_2 formation decreased, with increasing partial pressure of CO_2. It was confirmed that reverse water-gas shift reaction took place over Cr-MCM-41 by a separate experiment. The rate of CO formation during the dehydrogenation of ethylbenzene with CO_2 over Cr-MCM-41 was well accounted for by assuming parallel occurrence of two reactions, i.e., direct oxidative dehydrogenation of ethylbenzene with CO_2 and simple dehydrogenation of ethylbenzene thermodynamically assisted by reverse water-gas shift reaction.

1. Introduction

Styrene is one of the most important basic chemicals as a monomer of synthetic polymers. It is commercially produced by the dehydrogenation of ethylbenzene on the promoted iron oxide catalysts in the presence of a large quantity of steam at high temperatures of 600–700 °C, just below the temperature where the thermal cracking becomes significant. Due to its high endothermic and volume increasing character, a large amount of superheated steam is used to supply heat, lower the partial pressure of the reactants to shift the equilibrium to styrene, and avoid the formation of carbona-

ceous deposits to preserve the catalytic activity [1]. However, it has been pointed out that the preset commercial processes waste a large amount of latent heat of steam condensation at a liquid–gas separator following a reactor. Recently, CO_2 has received much attention as a co-feed gas for the dehydrogenation, because it is always gaseous throughout the dehydrogenation process. Moreover, reaction coupling is an effective approach to improve the equilibrium conversion in the dehydrogenation reactions [2]. Several investigations on reaction coupling were carried out in the dehydrogenation of ethylbenzene in the presence of carbon dioxide instead of steam [1,3–15], namely processes combined the ethylbenzene dehydrogenation with reverse water-gas shift reaction. It is estimated that the energy required for producing styrene is 6.3×10^8 cal/t in the coupling processes, only

42% of 1.5×10^9 cal/t in the current commercial process [3]. Therefore, such new processes that could be energy saving and environmentally friendly have been attracting more and more attention. Since Fe–K based catalysts used for present commercial dehydrogenation processes do not work effectively in the presence of CO_2, high performance catalysts have been screened extensively and some new catalysts were reported for the dehydrogenation of ethylbenzene in the presence of CO_2 [3–15]. An Fe_2O_3/Al_2O_3 catalyst prepared by co-precipitation [3,4], activated carbon-supported iron oxide [5,6,10], and mixed oxide catalysts prepared from hydrotalcite precursors, i.e., Mg–Al–Fe oxide [7], Li–Fe (Al) oxide [8], and Mg–Zn–Al–Fe oxide [9], have been proposed as active iron catalysts, whereas activated carbon-supported vanadium oxide [10], MgO-supported vanadium oxide [12], Al_2O_3 supported V–Sb mixed oxide [13,14], and Mg–V–Al mixed oxides prepared from hydrotalcite precursors [15] have been tested as vanadium catalysts.

Silica- and alumina-supported chromium oxides were industrially used for the productions of lower alkenes such as ethene, propene and isobutene through the dehydrogenation of the corresponding alkanes [16,17]. Carbon dioxide was found to enhance the dehydrogenation of ethane [18–20], propane [21–26] or isobutane [27] over supported chromium oxide. The reduction–oxidation property and the appropriate dispersion of chromium species on the support are important in these catalytic reactions [28,29]. MCM-41, a typical mesoporous molecular sieve, possesses uniform and well-ordered mesoporous channels with controllable pore size from 2 to 10 nm as well as high surface area (ca. $1000 \, m^2 \, g^{-1}$) [30], and thus could be used as a promising catalyst support. Studies of chromium species introduced into MCM-41 would thus be useful in developing Cr-containing catalysts with desirable catalytic properties. There exist several studies on the synthesis and characterizations of Cr-MCM-41 [31–35].

In the dehydrogenation of propane over Cr-MCM-41 catalysts prepared by direct hydrothermal synthesis (DHT), the selectivity to propene was higher than 90% with the yield of 30% and the presence of carbon dioxide enhanced propane conversion [36,37]. We have carefully studied on the structures of Cr-MCM-41 prepared by direct hydrothermal synthesis by X-ray diffraction, N_2 adsorption, diffuse reflectance UV–vis, X-ray absorption (XANES and EXAFS), and UV-Raman spectroscopic measurements. It was suggested that monochromate species mainly exist on the Cr-MCM-41 and are reduced to aggregated Cr(III) with octahedral coordination during the dehydrogenation reactions [38].

In the present paper, we report the catalytic behavior of Cr-MCM-41 in the dehydrogenation of ethylbenzene by carbon dioxide. The catalytic activities for both dehydrogenation and reverse water-gas shift reaction were tested and, moreover, regeneration of the deactivated catalyst by oxygen or carbon dioxide was investigated to elucidate the structure–activity relationships for the Cr-MCM-41 catalysts.

2. Experiment

2.1. Catalyst preparation

Various metals (M = Cr, Ga, V, and Fe) were introduced into MCM-41 by direct hydrothermal synthesis. Metal nitrate, sodium silicate, and hexadecyltrimethylammonium bromide were used as the sources of chromium and silicon, and the template, respectively. The molar ratio of the template to the silicon was kept at 0.5 in the synthesis gel. The synthesis gel was stirred for 1 h at room temperature and then transferred to a Teflon bottle, which was placed in a stainless-steel autoclave after the adjustment of the pH value of the mixed gel to 10.5 with 4 M HCl. The hydrothermal synthesis was carried out at 150 °C for 48 h, and then the resultant solid was recovered by filtration, washed thoroughly with deionized water, and dried at 40 °C in vacuum for ca. 24 h. After calcination at 550 °C for 6 h in a flow of dry air, M-MCM-41 was obtained. Cr-MCM-41 catalysts were prepared by changing the ratio of Cr to Si. As a control, Cr/Cab-O-Sil catalyst was prepared by impregnation of nonporous Cab-O-Sil (M5, Acros Organics) with Cr(III) nitrate.

2.2. Characterizations of catalysts

Inductively coupled plasma (ICP) optical emission spectroscopy was used for the determination of the metal content in each sample synthesized above. The measurements were performed with a Perkin-Elmer OPTIMA 3000, and the sample was dissolved in a mixture of HF and HNO_3 before the measurements.

N_2-adsorption studies were used to examine the porous properties of each sample. The measurements were carried out on a Belsorp 18SP equipment (volumetric), and all the samples were pretreated in vacuum at 200 °C for 12 h before the measurements. The pore-size distribution was evaluated from the adsorption isotherm by the Dollimore and Heal (DH) method [39].

X-ray diffraction (XRD) patterns were collected on a SRA M18XHF diffractometer (MAC Science Co., Ltd., Japan) with Cu Kα radiation (40 kV, 300 mA). Small divergent and scattering slits (0.05 mm) were selected to avoid a high background at low diffraction angles.

X-ray absorption spectroscopic measurements were performed with synchrotron radiation at a beam line BL7C station of Photon Factory, at the High Energy Accelerator Research Organization (Tsukuba, Japan), operated at 2.5 GeV with about 350–380 mA of ring current. The data were recorded in the X-ray fluorescence mode at room temperature using a Si(1 1 1) double crystal monochromator. Energy was calibrated with CuK-edge absorption (8981.0 eV), and the energy step of measurement in the XANES region was 0.3 eV. The absorption was normalized to 1.0 at an energy position of 30 eV higher than the absorption edge. Data reductions were performed with the FACOM M1800 computer system of the Data Processing Center of Kyoto University [40].

Diffuse reflectance UV–vis spectroscopic measurements were recorded on a JASCO UV/VIS/NIR (V-570) spectrophotometer. The spectra were collected in the range of 200–700 nm referenced to $BaSO_4$. The sample was loaded in an in situ cell and was treated in a pure N_2 gas flow at 200 °C for dehydration before the measurement.

Temperature-programmed oxidation (TPO) of the catalysts was carried out in a U-shaped quartz reactor. One hundred and fifty milligrams of the catalyst after the dehydrogenation of ethylbenzene at 550 °C for 1 h was used to determine the amount of carbon deposit on the catalyst. The temperature was increased up to 800 °C at a rate of 2.5 °C min^{-1} in a mixture of O_2 (5 ml min^{-1}) and N_2 (20 ml min^{-1}).

2.3. Catalytic reaction

The dehydrogenation of ethylbenzene was conducted using a fixed-bed flow reactor at atmospheric pressure. A quartz glass tube with an inner diameter of 8 mm was used as a reactor. In the dehydrogenation reactions, typically 0.15 g of catalyst, which had been pelletized and crushed to the particles 250–417 μm in diameter, was loaded into the reactor and treated in a gas flow containing N_2 (10 ml min^{-1}) and O_2 (10 ml min^{-1}) at 550 °C for 1 h and then purged with N_2. The reaction was started by introducing a gas mixture of ethylbenzene, N_2 and either CO_2 or Ar to the reactor. Ethylbenzene (0.6 ml min^{-1}; ca. 1.5 mmol h^{-1}) was fed by bubbling a gas mixture of CO_2 or Ar (30 ml min^{-1}) and N_2 (10 ml min^{-1}) through liquid ethylbenzene held at 28.3 °C in a thermostat. Ethylbenzene and the reaction products (styrene, toluene, and benzene) were liquefied with a cold trap of n-heptane and acetone at 0 °C, and analyzed by an FID gas chromatograph using a packed ID-BPX 5 column and cyclohexanone as an internal standard. Analyses of gaseous products (CO, CO_2, N_2, and H_2) were performed by a TCD gas chromatograph using a packed Molecular Sieve-5A column and Porapak Q. All the lines and valves between the cold trap and the reactor were heated to 150 °C to prevent the condensation of the partial oxidation products. The other hydrocarbons and the oxygenates were checked by a GC with FID using a packed

FFAP column, but were not detected. All data of the reactions were collected after the reaction for 1 h and used for the calculation of the reaction rates unless specifically mentioned, since the activity of the catalyst gradually decreased during the reaction.

3. Results and discussion

3.1. Properties of various M-MCM-41

Physical properties of supported metal catalysts are shown in Table 1. Metal contents determined by ICP analyses indicated that all the metals in starting gel were not fully incorporated in silica structure. V, Ga, and Fe-MCM-41 showed slightly larger surface area, pore volume, and pore diameter than Cr-MCM-41. When the Cr loading was changed, pore diameter was kept constant at 2.7 nm up to the Si/Cr ratio of 50, even though both pore volume and surface area decreased with increasing Cr content. Cr/Cab-O-Sil showed a smaller surface area compared with Cr-MCM-41 and the pore volumes of both Cab-O-Sil and Cr/Cab-O-Sil were negligibly small. While MCM-41 was white, as synthesized the color of Cr-MCM-41 was pale green and changed to pale yellow or yellow after the calcination at 550 °C for 6 h. XRD patterns at low diffraction angles showed four diffraction lines at 2θ of ca. 2.2°, 3.6°, 4.3°, and 5.7° indexed to (1 0 0), (1 1 0), (2 0 0), and (2 1 0) of the regularity of hexagonal array of mesopores of MCM-41 for all the samples. The peak intensities for the Cr-MCM-41 samples were not significantly lowered as compared with those for the purely silicious MCM-41, suggesting that the long-range regularity of hexagonal arrays of mesopores of MCM-41 was sustained after the introduction of chromium up to a content of 1.7 wt.% (Si/Cr = 50). However, as Si/Cr ratio decreased to 25 (3.4 wt.% of the Cr content), these diffraction peaks significantly decreased, indicating a decrease in the structural regularity of the mesoporous structure at higher Cr contents. This was clearly seen also in the drop in pore volume and surface area at the Si/Cr ratio of 25 (Table 1).

Table 1
Physical properties of supported metal catalysts

Catalyst	Si/M[a]	Si/M[b]	Surface area (m^2 g_{cat}^{-1})	Pore volume (cm^3 g_{cat}^{-1})	Pore diameter (nm)	Color	
						As-synthesized	Calcined
MCM-41	–	–	1025	0.94	2.7	White	White
Cr-MCM-41	100	165	878	0.79	2.7	Pale green	Pale yellow
	75	91	829	0.72	2.7	Pale green	Pale yellow
	50	57	780	0.70	2.7	Pale green	Yellow
	25	23	629	0.36	2.7	Pale green	Yellow
V-MCM-41	50	40	890	0.85	3.0	White	Pale orange
Ga-MCM-41	50	46	929	0.84	3.0	White	White
Fe-MCM-41	50	51	1016	0.75	3.0	White	Off white
Cr/Cab-O-Sil	50	55	163	–	–	Pale blue	Green
Cab-O-Sil	–	–	176	–	–	White	White

[a] Ratio of Si to metal calculated from the amounts of raw materials used.
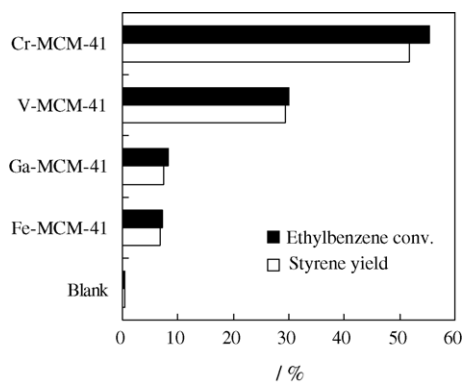[b] Ratio of Si to metal measured by ICP.

Fig. 1. The activities of various metals supported on MCM-41 (Si/M = 50). Catalyst: 0.15 g; N_2/CO_2: 10/30 ml min^{-1}; ethylbenzene: 1.5 mmol h^{-1}; reaction temperature: 550 °C; reaction time: 1 h.
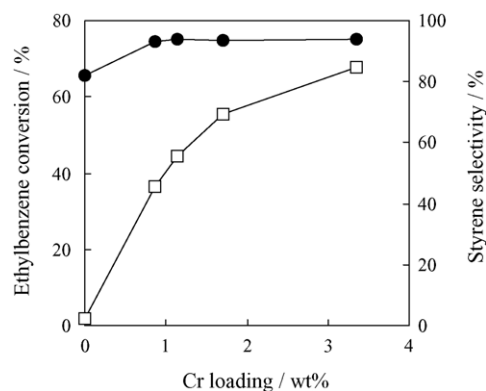

Fig. 2. Effect of Cr loading on the dehydrogenation of ethylbenzene with CO_2 over Cr-MCM-41. (□) Ethylbenzene conversion; (●) styrene selectivity. Catalyst: 0.15 g; N_2/CO_2: 10/30 ml min^{-1}; ethylbenzene: 1.5 mmol h^{-1}; reaction temperature: 550 °C; reaction time: 1 h.

3.2. Activities of various M-MCM-41

Effects of metal species were tested by using Cr (57), V (40), Ga (46), and Fe (51) on MCM-41 prepared by direct hydrothermal synthesis (number in the parenthesis shows the Si/M ratio determined by ICP), among which Cr-MCM-41 showed the highest activity, followed by V, Ga, and Fe supported on MCM-41 in the CO_2 dehydrogenation of ethylbenzene (Fig. 1). Cr-MCM-41 showed a yield of 52% with a high selectivity above 90% of styrene. The order of the activities of these metals almost coincided with those observed over both M-MCM-41 [37,38] and diamond-supported metal catalysts [22] in the propane dehydrogenation.

The selectivity to styrene is shown in Table 2 together with those to toluene and benzene as by-products. Higher selectivity to styrene together with higher conversion of ethylbenzene was observed over Cr-MCM-41 under the CO_2 atmosphere compared with Ar atmosphere. Under Ar atmosphere, benzene formation was enhanced in particular, whereas styrene formation was suppressed, suggesting that cracking of ethylbenzene was accelerated. Over Cr/Cab-O-Sil, styrene selectivity was always high above 95% under both CO_2 and Ar, but ethylbenzene conversion was lower than over Cr-MCM-41.

3.3. Behaviors of Cr-MCM-41

Effect of the Cr loading on Cr-MCM-41 on the dehydrogenation of ethylbenzene with CO_2 is shown in Fig. 2. Ethyl-

benzene conversion increased with increasing Cr content up to 1.7 wt.% (Si/Cr = 50), where the long-range regularity of hexagonal arrays of mesopores of MCM-41 was sustained after the introduction of chromium. Further increase in the Cr content resulted in a gradual increase in the activity, which is probably related to a change in the structure around Cr species. It is considered that, at higher Cr contents, the dispersion of Cr species decreased by the aggregation (vide infra) partly due to the decrease in the structural regularity of the mesoporous structure. The selectivity to styrene was low on MCM-41 without Cr and showed almost constant values above 90% over all Cr-MCM-41 irrespective of the Cr content.

Influence of the reaction temperature on the ethylbenzene dehydrogenation over Cr-MCM-41 (Si/Cr = 50) is shown in Fig. 3. With increasing the temperature up to 600 °C, ethylbenzene conversion linearly increased, while the selectivity to styrene gradually decreased. Further increase in the temperature caused a clear decrease in the selectivity to styrene. Benzene formation was significantly enhanced above 600 °C, suggesting that cracking of ethylbenzene was accelerated at the high temperature. Effect of contact time on the rates of both benzene and toluene formations in the ethylbenzene dehydrogenation over Cr-MCM-41 (Si/Cr = 50) at 550 °C is shown in Fig. 4. When the contact time was decreased to zero, the rate of toluene formation linearly decreased and closed to zero, whereas the rate of benzene formation still showed

Table 2
Dehydrogenation of ethylbenzene with CO_2 over supported Cr catalysts[a]

Catalyst[b]	Surface area (m^2 g$_{cat}^{-1}$)	Atmosphere	Conv. ethylbenzene (%)	Selectivity (%)		
				Styrene	Toluene	Benzene
Cr-MCM-41	780	CO_2	55.4	93.3	1.2	5.5
		Ar	38.6	85.1	1.5	13.3
Cr/Cab-O-Sil	163	CO_2	46.8	95.8	0.9	3.3
		Ar	31.3	95.9	0.0	4.1

[a] Catalyst: 0.15 g; N_2/CO_2: 10/30 ml min^{-1}; ethylbenzene: 1.5 mmol h^{-1}; reaction temperature: 550 °C; reaction time: 1 h.
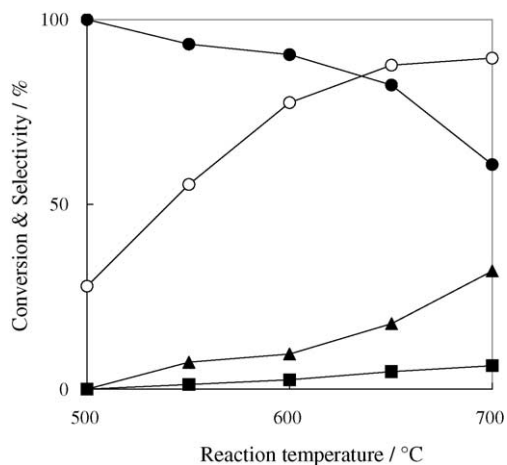[b] Si/Cr = 50.

Fig. 3. Effect of reaction temperature on the dehydrogenation of ethylbenzene with CO_2 over Cr-MCM-41 (Si/Cr = 50). (○) Ethylbenzene conversion; (●) styrene selectivity; (■) toluene selectivity; (▲) benzene selectivity. Catalyst: 0.15 g; N_2/CO_2: 10/30 ml min^{-1}; ethylbenzene: 1.5 mmol h^{-1}; reaction time: 1 h.

a certain positive value even at zero contact time, i.e., in the absence of the catalyst. With decreasing contact time, the selectivity to benzene increased to reach 53.4% while that to toluene decreased to 0% at zero contact time. No significant effect of the contact time on the selectivity to styrene was observed; the high values above 90% were always held except for the value of 46.6% at zero contact time. These results strongly suggest that the Cr-MCM-41 catalyst is indispensable for the styrene formation and, moreover, benzene is produced by thermal cracking reaction, whereas toluene forms by catalytic cracking over Cr-MCM-41 (Si/Cr = 50). The thermal cracking to benzene was supported by the result that the formation of benzene was more significantly accelerated than that of toluene with increasing reaction temperature (Fig. 3). Sugino et al. [6] reported that cracking of ethylbenzene to benzene and toluene occurred with a low selectivity of
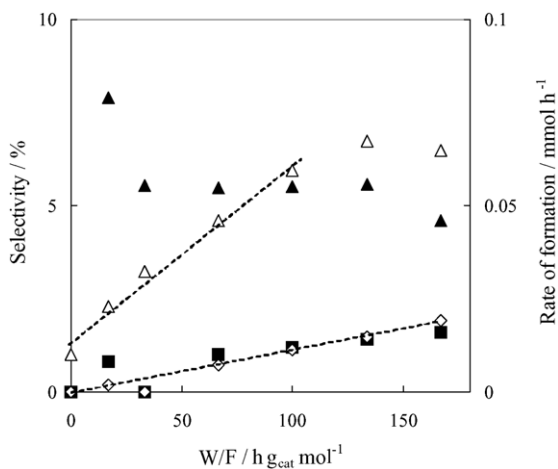

Fig. 4. Effect of W/F on the dehydrogenation of ethylbenzene with CO_2. (△) Rate of benzene formation; (◇) rate of toluene formation; (■) toluene selectivity; (▲) benzene selectivity. Reaction temperature: 550 °C.
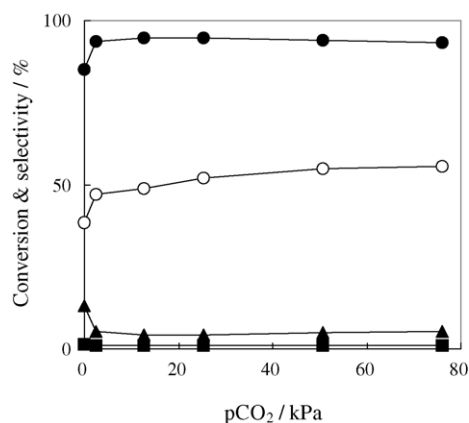
0.5–1.0% in the CO_2 dehydrogenation over an active carbon-supported iron catalyst (Fe 17 wt.%) at 500–700 °C. However, the amounts of these products were not large enough to account for the decrease in the selectivity to styrene. These results indicate that the decrease in the selectivity to styrene could be accounted for by thermal decomposition of ethylbenzene and styrene to coke over the Fe catalyst. Over the Cr-MCM-41 (Si/Cr = 50) catalyst in the present work, on the other hand, the formations of both benzene and toluene were more evident, whereas coke formation was negligibly small, compared with the reaction on the Fe catalyst. Benzene and toluene formed with the selectivity above 5 and 1%, respectively, suggesting that dehydrogenation to styrene was accompanied by thermal and catalytic cracking of ethylbenzene or reaction intermediates. It is likely that a part of benzene forms directly from ethylbenzene by thermal cracking, whereas toluene mainly forms via catalytic C–C bond fission from ethylbenzene or styrene over the catalyst.

3.4. Role of reverse water-gas shift reaction

Influence of partial pressure of CO_2 on the dehydrogenation of ethylbenzene over Cr-MCM-41 (Si/Cr = 50) is shown in Figs. 5 and 6. As seen in Fig. 5, both conversion of ethylbenzene and selectivity to styrene increased whereas selectivity to both benzene and toluene decreased by co-feeding CO_2 even at 2 kPa in the ethylbenzene/N_2 system. Further increase in the CO_2 pressure caused a slow increase in the ethylbenzene conversion, while the selectivities to styrene, benzene, and toluene showed no significant change. Rate of styrene formation revealed almost similar behavior to the ethylbenzene conversion, i.e., a quick increase by co-feeding CO_2 at 2 kPa followed by a gradual increase with further increase in the CO_2 pressure (Fig. 6). In the absence of CO_2, the production rate of H_2 and that of styrene coincided well with each other, suggesting that simple dehydrogenation of ethylben-

Fig. 5. Effect of partial pressure of CO_2 on the dehydrogenation of ethylbenzene over Cr-MCM-41 (Si/Cr = 50). (○) Ethylbenzene conversion; (●) styrene selectivity; (■) toluene selectivity; (▲) benzene selectivity. Catalyst: 0.15 g; ethylbenzene: 1.5 mmol h^{-1}; reaction temperature: 550 °C; reaction time: 1 h.
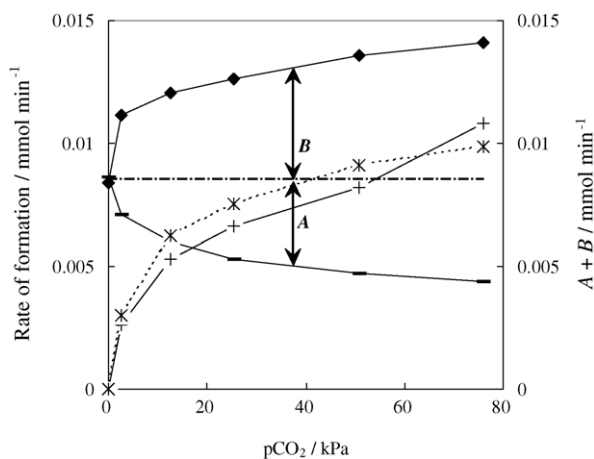
Fig. 6. Effect of partial pressure of CO_2 on the dehydrogenation of ethylbenzene with CO_2 over Cr-MCM-41 (Si/Cr = 50). (♦) Rate of styrene formation; (—) rate of H_2 formation; (+) rate of CO formation. *: A (increase in the rate of styrene formation) + B (decrease in the rate of H_2 formation). Catalyst: 0.15 g; ethylbenzene: 1.5 mmol h^{-1}; reaction temperature: 550 °C.

zene ((1), φ stands for a phenyl group) to styrene

$$\varphi\text{-}CH_2CH_3 \rightarrow \varphi\text{-}CH{=}CH_2 + H_2 \tag{1}$$
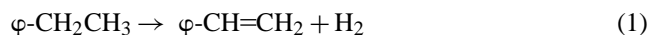
took place over Cr-MCM-41 (Si/Cr = 50). By co-feeding CO_2, the rate of H_2 production decreased whereas the rate of CO production increased, suggesting that reverse water-gas shift reaction (2) simultaneously took place over the catalyst. Actually, the

$$CO_2 + H_2 \rightarrow CO + H_2O \tag{2}$$

occurrence of the shift reaction (2) was confirmed by feeding a mixed gas of CO_2 and H_2 over Cr-MCM-41 (Si/Cr = 50) (Table 3). The amount of H_2 consumed well coincided with that of CO formed during the reaction, indicating that the shift reaction (2) occurred over Cr-MCM-41 (Si/Cr = 50).

Jóźwiak et al. [41] reported that, when Cr(VI)O_3 was supported on SiO_2 by an incipient-wetness method, a thermally stable chromate-like species Cr(VI)O_4^{2-} formed on the surface of the sample with the low Cr loading less than 3.0 wt.% after the calcination at 500 °C. These molecularly dispersed chromate species form in high population on silica surface and are anchored to silica substrate in the form of chromate esters (Fig. 7). The increase in Cr content leads gradually to di- or polychromate species, amorphous and finally crystalline α-chromia phases. These results well coincide with those observed for the surface structure of chromium oxides on Cr-MCM-41 catalysts by the authors [37,38]. We have pre-
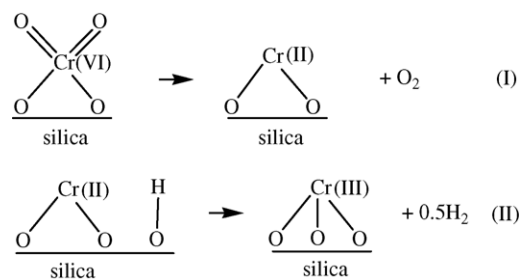

Fig. 7. Formation of active species on MCM-41.

pared Cr-MCM-41 starting from Cr(III) nitrate and observed the formation of Cr(VI)O_4 tetrahedra after the calcination at 550 °C. The isolated chromate species may lose two terminally bonded oxygen atoms by the recombination leading to the evolution of oxygen molecule as well as the formation of Cr(II)O_2^{2-} species (Fig. 7, Scheme I) [41]. In the presence of water, coordination of an extra OH group takes place, resulting in the Cr(II) oxidation to Cr(III) species (Fig. 7, Scheme II). On the CrO_x/silica with low Cr loading, reversible interconversions Cr(VI) ↔ Cr(III) and Cr(VI) ↔ Cr(II) seem to occur when hydrogen or carbon monoxide are used as the reducing agent [41].

It is frequently reported that water-gas shift reaction proceeds via a mechanism of reduction–oxidation of active metal species as seen in the behavior of CeO_2 in ceria-supported Pt, Pd, and Rh catalysts [42] and Cu- and Ni-loaded cerium oxide catalysts [43]. In these studies, a co-operative redox reaction mechanism, involving oxidation of CO adsorbed on the metal cluster by oxygen supplied to the metal interface by ceria, followed by H_2O capping the oxygen vacancy on ceria, well explained the results obtained by the kinetic studies. The Cr(II) and Cr(III) oxo species are often regarded as the catalytic sites on silica surface in many reactions [44–46]. Also in the present work, it is considered that reverse water-gas shift reaction may proceed through a coupling of Cr(III) reduction to Cr(II) by H_2 (3) and, inversely, Cr(II) oxidation to Cr(III) by CO_2 (4) over Cr-MCM-41:

$$Cr(III)\text{-}O^- + H_2 \rightarrow Cr(II) + H_2O \tag{3}$$

$$Cr(II) + CO_2 \rightarrow Cr(III)\text{-}O^- + CO \tag{4}$$
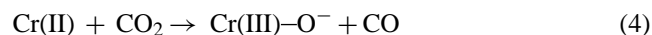
### 3.5. Direct contribution of CO_2

When this catalyst was applied in the system of ethylbenzene–CO_2, H_2 produced by the dehydrogenation (1) could be consumed by reverse water-gas shift reaction (2) and

Table 3
Reversed water-gas shift reaction over Cr-MCM-41 catalysts[a]

Reaction (time/h)	CO_2 (mmol min^{-1})	H_2 (mmol min^{-1})	H_2 consumption (mmol min^{-1})	CO formation (mmol min^{-1})
Feed gas	1.663	0.0716	–	–
0.5	1.638	0.0514	0.0202	0.0208

[a] Cr-MCM-41 (Si/Cr = 50): 400 mg; pre-treatment at 550 °C for 1 h under the mixed gas-flow of N_2/O_2 at 10/10 ml min^{-1}; reaction at 550 °C under the mixed gas-flow of N_2/CO_2/H_2 at 10/23/1 ml min^{-1}.

the thermodynamic equilibrium of the dehydrogenation (1) would shift toward styrene formation, resulting in an increase in the rate of styrene formation. Assuming that CO forms by reverse water-gas shift reaction (2), the rate of CO formation would be equal to a decrease in the rate of H_2 formation. The decrease in the rate of H_2 formation was calculated based on the rate obtained by simple dehydrogenation in the absence of CO_2 (Fig. 6A). As a result, the value was always ca. 45% of the rate of CO formation regardless of the CO_2 pressure up to 52 kPa. This suggests that the remaining part of CO (ca. 55%) evolved from reactions other than the reverse water-gas shift reaction. The sum of an increase in the rate of styrene formation (Fig. 6B) and a decrease in the rate of H_2 formation (Fig. 6A) is plotted against the partial pressure of CO_2. The sum value of A and B almost coincided with the rate of CO formation throughout all partial pressure of CO_2, indicating that the remaining part of CO mainly evolved accompanied by styrene formation. Moreover, judging from the logarithmic plot, the rate of ethylbenzene consumption showed a first order dependency on the partial pressure of CO_2, suggesting that CO_2 directly contributed to the dehydrogenation of ethylbenzene. A plausible mechanism of such direct contribution of CO_2 is that CO_2 works as the oxidizing agent of ethylbenzene to styrene (5):

$$\varphi\text{-}CH_2CH_3 + CO_2 \rightarrow \varphi\text{-}CH=CH_2 + CO + H_2O \qquad (5)$$
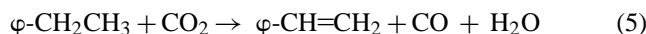
As shown in the results of CO_2 dehydrogenation of ethylbenzene over Cr-MCM-41 with various Cr loadings at 550 °C (Fig. 2), the selectivity to styrene was always higher than 90% and the conversion of ethylbenzene increased almost linearly with an increase in the Cr loading. Even though the BET surface area and pore volume greatly decreased as the Cr loading increased to 3.4 wt.% (Si/Cr = 25) (Table 1), the conversion of ethylbenzene and the yield of styrene increased with increasing Cr loading, indicating such change in the porous structure did not significantly influence the catalytic behavior. It has been clearly seen that the simple dehydrogenation of ethylbenzene took place over Cr-MCM-41 even in the absence of CO_2 (Fig. 5). The rate of styrene formation remarkably increased together with that of CO formation with increasing partial pressure of CO_2. According to thermodynamic equilibrium of dehydrogenation of ethylbenzene (1) at 550 °C in the gas mixture of ethylbenzene−Ar at the molar ratio of 1:2.5 and at WHSV = 0.2 h^{-1}, ethylbenzene conversion was calculated as 44.7% [47], almost coinciding with the value obtained in Fig. 5. According to the thermodynamic considerations [10], ethylbenzene conversion can be improved by coupling the reaction with reverse water-gas shift reaction (2). Moreover, the direct contribution of CO_2 (5) possibly shifts the dehydrogenation equilibrium towards products under CO_2 atmosphere. The results obtained in the present work, i.e., the increases in both ethylbenzene conversion and styrene yield in the presence of CO_2, are well explained by these considerations.
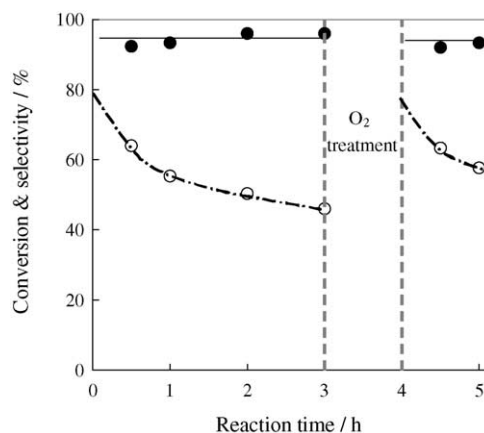

Fig. 8. Deactivation and regeneration of Cr-MCM-41 (Si/Cr = 50) during the dehydrogenation of ethylbenzene with CO_2. (○) Ethylbenzene conversion; (●) styrene selectivity. Catalyst: 0.15 g; N_2/CO_2: 10/30 ml min^{-1}; ethylbenzene: 1.5 mmol h^{-1}; reaction temperature: 550 °C.

3.6. Deactivation and regeneration of Cr-MCM-41

Cr-MCM-41 (Si/Cr = 50) showed the ethylbenzene conversion of 64.1% with the styrene yield of 59.1% with a gas mixture of N_2−CO_2-ethylbenzene at the molar ratio of 27/80/1.5 and at GHSV = 6800 ml g$_{cat}$$^{-1}$ h^{-1} at the reaction time of 0.5 h (Fig. 8). The activity gradually decreased during the reaction over Cr-MCM-41, indicating the occurrence of catalyst deactivation. After the reaction for 3 h, the gas-flow of the mixture of ethylbenzene and CO_2 was replaced by the mixed gas-flow of O_2/N_2 at the ratio of 10/10 ml min^{-1}. After the treatment with O_2 for 1 h, the reaction was restarted by replacing the gas flow with the mixture of ethylbenzene and CO_2. The activity of Cr-MCM-41 was recovered; both ethylbenzene conversion and styrene yield returned to the original values of 63.3 and 58.3%, respectively, after the treatment with O_2 (Fig. 8). When the catalyst was again put in the reaction conditions after the O_2 treatment, the conversion of ethylbenzene decreased in an almost similar way to the first reaction step.

In the XRD patterns for Cr-MCM-41 after the reactions, the peak intensities at the low diffraction angles significantly decreased under Ar atmosphere as compared with those under CO_2 atmosphere, suggesting that the long-range regularity of hexagonal arrays of mesopores of MCM-41 was weakened after the reaction in Ar. Both surface area and pore volume were also significantly decreased under Ar atmosphere, but were stable under CO_2 atmosphere. These suggest that lattice oxygen in Cr-MCM-41 was consumed during the dehydrogenation under Ar atmosphere, resulting in the collapse or the weakening of the long-range regularity of hexagonal arrays. On the other hand, the defect formed by the lattice oxygen uptake can be refilled by oxygen from gas phase CO_2, resulting in no substantial change in the structure under CO_2 atmosphere. XRD measurements showed no diffraction line assigned to any chromium species during all processes, i.e., the dehydrogenation reaction and the O_2 treatment.
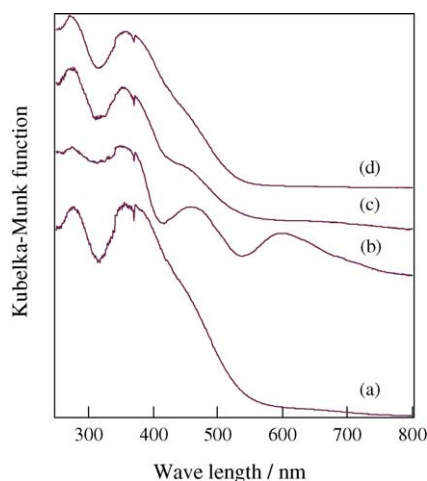
Fig. 9. Diffuse reflectance UV–vis spectra of Cr-MCM-41 (Si/Cr = 50): (a) fresh; (b) after the reaction for 3 h under CO_2; (c) after the reaction for 3 h under CO_2 followed by CO_2 treatment at 650 °C for 1 h; (d) after the reaction for 3 h under CO_2 followed by O_2 treatment at 550 °C for 1 h.

In the Cr K-edge XANES spectra of Cr-MCM-41, the change in the local symmetry around the chromium center from CrO_4 tetrahedral coordination to CrO_6 octahedral co-ordination was observed during the ethylbenzene dehydrogenation. Moreover, the results of Fourier transforms of k^3-weighted Cr K-edge EXAFS indicated that CrO_4 tetrahedra consists of two Cr=O bonds and two Cr–O bonds before the reaction, whereas both CrO_6 octahedra and Cr–O–Cr through corner-shared CrO_6 octahedra appeared to form small $Cr(III)O_x$ clusters after the dehydrogenation reaction. After the treatment with O_2, both XANES and EXAFS spectra showed that the $Cr(VI)O_4$ tetrahedra were regenerated by the reoxidation of the $Cr(III)O_6$ octahedra. These results obtained by both XRD and X-ray absorption spectroscopic measurements were almost similar to those observed in the dehydrogenation of propane [37,38].

Diffuse reflectance UV–vis spectra of Cr-MCM-41 (Si/Cr = 50) with the Si/Cr ratio of 50 during the reaction are shown in Fig. 9. UV bands at 280 and 370 nm, which could be assigned to O–Cr(VI) charge transfer of chromates species [37,38,48], were mainly observed together with a weak shoulder around 450 nm assigned to Cr(VI) polychromate for a fresh sample of Cr-MCM-41 (Fig. 9a). The bands at ca. 450 and 600 nm appeared after the dehydrogenation reaction with CO_2 for 1 h could be assigned to octahedral Cr(III) in Cr_2O_3 or CrO_x clusters, whereas the Cr(VI) species observed at 280 and 370 nm could be in tetrahedral coordination (Fig. 9b). No diffraction line of Cr_2O_3 was observed in XRD patterns of Cr-MCM-41 after the reaction, suggesting that Cr species are still well dispersed on Cr-MCM-41. It is concluded that tetrahedrally coordinated $Cr(VI)O_4$ exists on Cr-MCM-41 before the reaction (Fig. 9a) and reduced to octahedrally co-ordinated $Cr(III)O_6$ during the reaction (Fig. 9b). It is also noteworthy that the latter species appeared as polychromates on Cr-MCM-41, the sizes of which are too small to be ob-

served in XRD. Such change in both the coordination structure and valence state of chromium caused the deactivation of Cr-MCM-41. After the CO_2 treatment of the deactivated Cr-MCM-41 at 650 °C (Fig. 9c), the bands at 280 and 370 nm assigned to O–Cr(VI) charge transfer of tetrahedral CrO_4 were regenerated, whereas those at ca. 450 and 600 nm assigned to octahedral Cr(III) in Cr_2O_3 or CrO_x clusters disappeared even though a peak around 450 nm assigned to Cr(VI) polychromate was still observed as a shoulder. After the O_2 treatment at 550 °C, the latter shoulder was almost weakened and the original spectra observed for the fresh sample were regenerated, indicating that the O_2 treatment was effective in recovering the original coordination structure of the active chromium species (Fig. 9d).

3.7. Coke formation on Cr-MCM-41-DHT

Table 4 shows the coke amounts estimated by TPO measurement of the catalysts after the dehydrogenation reaction of ethylbenzene under CO_2 and Ar atmosphere at 550 °C for 1 h. On Cr-MCM-41 and Cr/Cab-O-Sil catalysts (both Si/Cr = 50), 0.60 and 0.31 wt.% of coke was formed under CO_2 atmosphere, respectively, while 0.38 and 0.13 wt.% of coke under Ar atmosphere, respectively; larger amounts of coke deposited on both catalysts under CO_2 atmosphere than under Ar atmosphere. Coke can be formed more intensively on the catalyst surface from styrene than from ethylbenzene, and therefore the enhanced formation of styrene over Cr-MCM-41 reasonably resulted in a larger amount of coke formation. It was clearly observed that CO was produced from CO_2 during the ethylbenzene dehydrogenation over Cr-MCM-41 (Si/Cr = 50) (Fig. 6). It must be noticed that CO_2 can be converted to CO via reverse water-gas shift reaction by consuming H_2 or via Boudouard reaction by consuming coke on the catalyst surface. The behavior of Cr-MCM-41 catalyst is similar to that of V_2O_5/MgO [12], on which CO_2 could not suppress the coke formation. It is likely that coke formed from styrene as a main product, the formation of which in high concentration possibly resulted in enhanced coke formation. The activity was quickly regenerated on Cr-MCM-41 even after the oxidation treatment for a short time, i.e., 1 h, during which, however, coke elimination was not completed. Such non-completed coke elimination was confirmed by GC analyses during the oxidation treatment, indicating

Table 4
Amount of carbon deposited on the catalyst during the reaction[a]

Catalyst	Reaction atmosphere	Carbon deposited (mg)
Cr-MCM-41 (Si/Cr = 50)	CO_2	0.90
	Ar	0.57
Cr/Cab-O-Sil (Si/Cr = 50)	CO_2	0.46
	Ar	0.20

[a] Each catalyst (150 mg) used for the dehydrogenation of ethylbenzene at 550 °C for 1 h was treated under a mixed gas-flow of O_2/N_2 (5/20 ml min^{-1}) at a rate of 2.5 °C min^{-1} from room temperature to 800 °C.

that the catalyst deactivation was not caused by the coke formation.

It seems that the tetrahedrally coordinated Cr(VI) plays an important role in the dehydrogenation of ethylbenzene with CO_2. However, the reaction proceeded under CO_2 atmosphere even after the deactivation, where Cr(VI) tetrahedra almost disappeared and moreover its quick regeneration was not easy. It is most likely that molecularly dispersed chromium species possess an important role in the catalysis for the ethylbenzene dehydrogenation with CO_2 probably by the redox cycle between Cr(II) and Cr(III) as suggested in the water-gas shift reaction.

4. Conclusion

Cr-MCM-41 catalysts prepared by direct hydrothermal synthesis showed high activity in the dehydrogenation of ethylbenzene with carbon dioxide, resulting in the production of styrene with the conversion of 65% and the selectivity above 90%. It is suggested that Cr(VI) in tetrahedral coordination formed as an active monochromate species and reduced to Cr(III) in octahedral coordination as a less active polychromate species during the reaction. The deactivated catalyst was regenerated by a treatment with gaseous oxygen, during which the reoxidation of the Cr(III) species to the Cr(VI) species was observed. Not only gaseous oxygen but also carbon dioxide could regenerate $Cr(VI)O_4$ tetrahedra from reduced $Cr(III)O_6$ octahedra, even though the efficiency of carbon dioxide was lower than that of oxygen. However the reaction still proceeded under CO_2 atmosphere even after the deactivation, where Cr(VI) tetrahedra almost disappeared. Moreover, reverse water-gas shift reaction was catalyzed over Cr-MCM-41, and the catalytic cycle is probably composed of the reduction–oxidation between Cr(III) and Cr(II) species. Hydrogen formed by the dehydrogenation of ethylbenzene was consumed by reverse water-gas shift reaction, resulting in the acceleration of ethylbenzene dehydrogenation. The rate of CO formation was well accounted for by two origins, i.e., one from the reverse water-gas shift reaction and the other from the direct oxidative dehydrogenation of ethylbenzene by CO_2. It is suggested that ethylbenzene is dehydrogenated to styrene directly with CO_2 and also coupled by reverse water-gas shift reaction and that both reactions were catalyzed by the reduction–oxidation cycle between Cr(III) and Cr(II).

References

[1] J. Matsui, T. Sodesawa, F. Nozaki, Appl. Catal. A 67 (1991) 179.
[2] G. Towler, S. Lynn, Chem. Eng. Sci. 49 (1994) 2585.
[3] N. Miura, M. Saito, Catal. Today 55 (2000) 173.
[4] M. Saito, H. Kimura, N. Mimura, J. Wu, K. Murata, Appl. Catal. A 239 (2003) 71.
[5] T. Badstube, H. Papp, R. Dziembaj, P. Kustrowski, Appl. Catal. A 204 (2000) 153.
[6] M. Sugino, H. Shimada, T. Turuda, H. Miura, N. Ikenaga, T. Suzuki, Appl. Catal. A 121 (1995) 125.
[7] P. Kustrowski, A. Rafalska-Lasocha, D. Majda, D. Tomaszewska, R. Dziembaj, Solid State Ion. 141–142 (2001) 237.
[8] R. Dziembaj, P. Kustrowski, L. Chmielarz, Appl. Catal. A 255 (2003) 35.
[9] X. Ye, N. Ma, W. Hua, Y. Yue, C. Miao, Z. Xie, Z. Gao, J. Mol. Catal. A 217 (2004) 103.
[10] A. Sun, Z. Qin, J. Wang, Appl. Catal. A 234 (2002) 179.
[11] A. Sun, Z. Qin, S. Chen, J. Wang, J. Mol. Catal. A 210 (2004) 189.
[12] Y. Sakurai, T. Suzaki, K. Nakagawa, N. Ikenaga, H. Aota, T. Suzuki, J. Catal. 209 (2002) 16.
[13] V.P. Vislovski, J.-S. Chang, M.-S. Park, S.-E. Park, Catal. Commun. 3 (2002) 227.
[14] M.-S. Park, V.P. Vislovski, J.-S. Chang, Y.-G. Shul, J.S. Yoo, S.-E. Park, Catal. Today 87 (2003) 205.
[15] G. Carja, R. Nakamura, T. Aida, H. Niiyama, J. Catal. 218 (2003) 104.
[16] L.R. Mentasty, O.F. Gorriz, L.E. Cadus, Ind. Eng. Chem. Res. 38 (1999) 389.
[17] A. Hakuli, M.E. Harlin, L.B. Backman, A.O.I. Krause, J. Catal. 184 (1999) 349.
[18] S. Wang, K. Murata, T. Hayakawa, S. Hamakawa, K. Suzuki, Appl. Catal. A 196 (2000) 1.
[19] X. Ge, M.M. Zhu, J.Y. Shen, React. Kinet. Catal. Lett. 77 (2002) 103.
[20] N. Mimura, I. Takahara, M. Inaba, M. Okamoto, K. Murata, Catal. Commun. 3 (2002) 257.
[21] I. Takahara, W.C. Chang, N. Nimura, M. Saito, Catal. Today 45 (1998) 55.
[22] K. Nakagawa, C. Kajita, N. Ikenaga, M. Nishitani-Gamo, T. Ando, T. Suzuki, Catal. Today 84 (2003) 149.
[23] S.M. Al-Zahrani, B.Y. Jibril, A.E. Abasaeed, Catal. Today 81 (2003) 507.
[24] M. Cherian, M.S. Rao, G. Deo, Catal. Today 78 (2003) 397.
[25] K.L. Fujdala, T.D. Tilley, J. Catal. 218 (2003) 123.
[26] M. Cherian, M.S. Rao, W.-T. Yang, J.-M. Jehng, A.M. Hirt, G. Deo, Appl. Catal. A 233 (2002) 21.
[27] P. Moriceau, B. Grzybowska, L. Gengembre, Y. Barbaux, Appl. Catal. A 199 (2000) 73.
[28] B. Crzybowska, J. Słoczyński, R. Grabowski, K. Wcisło, A. Kozłowska, J. Stoch, J. Zieliński, J. Catal. 178 (1998) 687.
[29] M. Cherian, M.S. Rao, A.M. Hirt, I.E. Wachs, G. Deo, J. Catal. 211 (2002) 482.
[30] C.T. Krege, M.E. Leonowicz, W.J. Roth, J.C. Vartuli, J.S. Beck, Nature 359 (1992) 710.
[31] D. Trong On, D. Desplantier-Giscard, C. Danumach, D. Kaliaguine, Appl. Catal. A 222 (2001) 299.
[32] N. Ulagappon, C.N.R. Rao, Chem. Commun. (1996) 1047.
[33] W. Zhang, T.J. Pinnavaia, Catal. Lett. 38 (1996) 261.
[34] Z. Zhu, Z. Zhang, L. Kevan, J. Phys. Chem. B 103 (1999) 2680.
[35] J.S. Gonzalez, J.M. Robles, M.A. Rodriguez, P.M. Torres, E.R. Castellon, A.J. Lopez, Catal. Lett. 64 (2000) 209.
[36] Y. Wang, Q. Zhang, Q. Guo, T. Chen, H. Wan, Y. Ohishi, T. Shishido, K. Takehira, Chem. Lett. 11 (2002) 1152.
[37] Y. Wang, Y. Ohishi, T. Shishido, Q. Zhang, W. Yang, Q. Guo, H. Wan, K. Takehira, J. Catal. 220 (2003) 347.
[38] K. Takehira, Y. Ohishi, T. Shishido, T. Kawabata, K. Takaki, Q. Zhang, Y. Wang, J. Catal. 224 (2004) 404.
[39] D. Dollimore, G.R. Heal, J. Appl. Chem. 14 (1964) 109.
[40] K. Tanaka, H. Yamashita, R. Tsuchitani, T. Funabiki, T. Yoshida, J. Chem. Soc., Faraday Trans. 84 (1988) 2987.
[41] W.K. Jóźwiak, W. Ignaczak, D. Dominiak, T.P. Maniecki, Appl. Catal. A 258 (2004) 33.
[42] T. Bunluesin, R.J. Gorte, G.W. Graham, Appl. Catal. B 15 (1998) 107.

[43] Y. Li, Q. Fu, M. Flytzani-Stephanopoulos, Appl. Catal. B 27 (2000) 179.
[44] M.P. McDaniel, M.M. Johnson, J. Catal. 101 (1986) 446.
[45] W.K. Jóźwiak, I.G. Dalla Lana, J. Chem. Soc., Faraday Trans. 93 (1997) 2583.
[46] M.P. McDaniel, Adv. Catal. 33 (1985) 47.
[47] N.S. Nesterenko, O.A. Ponomoreva, V.V. Yuschenko, I.I. Ivanova, F. Testa, F. Di Renzo, F. Fajula, Appl. Catal. A 254 (2003) 261.
[48] B.M. Weckhuyen, I.E. Wachs, R.A. Schoonheydt, Chem. Rev. 96 (1996) 3327.